J Nanopart Res (2014) 16:2316
DOI 10.1007/s11051-014-2316-3

RESEARCH PAPER

The effect of SiO_2 shell thickness on the magnetic properties of $ZnFe_2O_4$ nanoparticles

Mustafa Coşkun · Mustafa Korkmaz

Received: 12 July 2013 / Accepted: 4 February 2014 / Published online: 22 February 2014

Abstract We have analyzed the magnetic properties of oleic acid (OA)-coated and SiO_2-coated $ZnFe_2O_4$ nanoparticles. OA-coated $ZnFe_2O_4$ nanoparticles were synthesized by a normal micelles process using OA as a capping agent, and SiO_2-coated $ZnFe_2O_4$ nanoparticles with controlled SiO_2 shell thicknesses were prepared by a base-catalyzed silica formation from tetraethylorthosilicate (TEOS) in a water-in-oil microemulsion using OA-coated $ZnFe_2O_4$ nanoparticles as seeds. The structure, morphology, and particle size of synthesized ferrite nanoparticles were characterized by X-ray powder diffractometry (XRD) and transmission electron microscopy (TEM). Magnetic properties of samples were carried out with a physical property measurement system and electron paramagnetic resonance spectroscopy. From XRD analysis, it was concluded that the prepared $ZnFe_2O_4$ nanoparticles had a single-ferrite phase. TEM analysis revealed that the formation of OA-coated $ZnFe_2O_4$ nanoparticles with a narrow-size distribution in the range of 5.0–6.5 nm and with the SiO_2 thickness attaining up to 14.0 nm approximately in TEOS content increases from 0.25 to 2.5 mL during the process. The results of the magnetic measurements indicated that some magnetic properties of the SiO_2-coated particles have been changed compared with OA-coated particles due to decrease in the interparticle magnetic interactions between $ZnFe_2O_4$ nanoparticles passivated by coating with SiO_2 shells of various thicknesses.

Keywords Magnetic nanoparticles · SiO_2 coating · Electron paramagnetic resonance (EPR) · Dipolar interaction · Nanoparticle interactions

M. Coşkun (✉) · M. Korkmaz
Department of Physics Engineering, Hacettepe University, Beytepe, 06800 Ankara, Turkey
e-mail: mcoskun@hacettepe.edu.tr

Introduction

In recent years, the magnetic nanoparticles have drawn much research attention due to their unique magnetic properties originating from their small size (Lu et al. 2007). Among various magnetic nanoparticles, ferrite nanoparticles have become exceptionally popular for a wide variety of applications such as magnetic recording equipment (Han et al. 1996), magnetic fluids (Lopez et al. 2012), drug delivery (Wang et al. 2011), and hyperthermia treatment (Kim et al. 2010) applications. Ferrites, which adopt cubic spinel structures and have a general formula of $[A][B]_2O_4$, where [A] and [B] indicate tetrahedral and octahedral cation sites, respectively, are very important classes of magnetic materials. Their magnetic and electronic properties are determined by their crystal structure and chemical compositions and, in particular, by the location of divalent metal ions and iron between the oxygen ions (Carter and Norton 2007). Among the ferrite nanoparticles, $ZnFe_2O_4$ nanoparticles have

attracted a great deal of research interest due to their unusual magnetic properties that are different from the bulk ones. Bulk $ZnFe_2O_4$ has a normal spinel structure with Zn^{2+} ions in the A-site and Fe^{3+} ions in the B-sites (Tung et al. 2002). However, nanocrystalline $ZnFe_2O_4$ system always shows up as a mixed spinel in which Zn^{2+} and Fe^{3+} ions are distributed over the A- and B-sites and exhibits anomaly in its magnetization (Xu et al. 2011; Deraz and Alarifi 2012).

Due to the potential applications of ferrite nanoparticles, a wide variety synthesis process for the production of nanoparticles have been developed including sol–gel (Gatelyte et al. 2011), ball milling (Chakka et al. 2006), solvothermal (Yanez-Vilar et al. 2009), hydrothermal (Nalbandian et al. 2008), and microemulsion (Moumen and Pileni 1996). Since most of these colloidal nanoparticles are synthesized in organic solvents using hydrophobic capping reagents, they are dispersible only in hydrophobic organic solvents. In addition, the organic capping layers can decompose, and the metal nanoparticles can deform and aggregate above 300 °C temperatures (Joo et al. 2009). However, the possible biological applications of these nanoparticles are greatly restricted because of their poor dispersibility in aqueous solutions. One method for compatibility in biological system and high dispersibility under different solutions is to coat the particles, which means to create a water-dispersible core/shell structure. These core/shell nanoparticles have core made of a material coated with water compatible shell.

Coated nanoparticles have become an active field because of their unique chemical, optical, electronic, magnetic properties, and potential applications in many areas compared to those of non-core/shell nanoparticles (Madrakian et al. 2012; Selvan 2010; Ghiaci et al. 2012). In order to synthesize core/shell nanoparticles, many different chemical methods have been developed such as chemical precipitation (Bayal and Jeevanandam 2012), sol–gel (Wu et al. 2012), microemulsion (Wang et al. 2010), and inverse micelles (Lee et al. 2008). To prevent oxidation and magnetic aggregations, nanoparticles are often coated with organic surfactants (Ma et al. 2012), gold (Ahmad et al. 2012), SiO_2 (Coskun et al. 2012), and polymers (Quarta et al. 2012). An inert shell encapsulating the surface of the nanoparticles screens the magnetic dipolar attraction and prevents direct contact between the particles (Lu et al. 2007; Quarta et al. 2012; Coskun et al. 2010). In addition, the core/shell structure enhances the thermal and chemical stability of nanoparticles regarding to the chemically inert shell especially in biological systems. SiO_2 is one of the non-toxic, water-dispersible, and biocompatible material to coat core structure of the nanoparticles. SiO_2 shell provides a chemically inert surface for magnetic nanoparticles in biological systems and allows to conjugate its surface with various functional groups (Deng et al. 2005; Soundarya and Zhang 2010). Stöber (Kobayashi et al. 2005) and reverse micelle methods (Hagura et al. 2010) are the two main process for SiO_2 coating the nanoparticles in the literature.

In this manuscript, we reported a detailed comparative study of oleic acid (OA) and SiO_2 coating onto $ZnFe_2O_4$ nanoparticles based on the characterization for their possible usage in biomedical research and diagnostics. The synthesis is based on a two-step method: (i) synthesis of OAcapped $ZnFe_2O_4$ core using a solution process, and (ii) SiO_2 coating on the core by the inverse microemulsion technique. Nanoparticles prepared by this two-step method were characterized by XRD, TEM, VSM, and electron paramagnetic resonance (EPR) techniques.

Experimental

OA-coated $ZnFe_2O_4$ nanoparticles were synthesized via chemical route developed by Caruntu et al. (2002, 2004, 2007). Briefly, 10 mmol of $FeCl_3{\cdot}6H_2O$ (97 %), 5 mmol of $ZnCl_2$ (97 %), 250 mL of DEG (99 %), and 40 mmol of sodium hydroxide (NaOH) (97 %) were combined with solution into a three neck flask at room temperature under a N_2 flow with vigorous stirring. The solution was heated to 230 °C for 2 h, and then 8 mmol of OA (95 %) was added to the solution. The black colored product was separated via centrifugation at 5,000 rpm for 20 min. The sample was washed three times in absolute ethanol and then dried in N_2 atmosphere. The average diameter of the ferrite nanoparticles was 5.75 nm with a narrow-size distribution as determined by TEM. The thickness of OA layer is approximately in the size of an OA molecule (1–1.2 nm), as was determined by Murai et al. (2007).

Tetraethylorthosilicate (TEOS) was used to coat the ferrite nanoparticles by a base-catalyzed silica formation water-in-oil microemulsion. The details of the process were reported elsewhere (Lee et al. 2006). In brief, 8 mL of Igepal CO-520 was mixed with cyclohexane (175 mL) under vigorous stirring at room

temperature for 20 min. OA-coated ferrite nanoparticles were dispersed in cyclohexane at a concentration of 1 mg/mL and slowly added to the Igepal CO-520/cyclohexane mixture and vortexed for 3 h. An aqueous ammonia solution (28 wt%) was added dropwise and stirred for 5 min. Finally, TEOS was slowly dropped into the mixture. Depending on the desired SiO_2 shell thickness, the amount of added TEOS was varied from 0.25 to 2.5 mL. The coating reaction proceeded at 30 °C for 72 h under vigorously stirring before the addition of ethanol to precipitate the nanoparticles. Finally, SiO_2-coated nanoparticles were collected by centrifugation and washed at least three times to remove unreacted organic chemicals, and then dried at 30 °C for 6 h.

XRD measurements were performed on a powder sample of OA- and SiO_2-coated $ZnFe_2O_4$ nanoparticles using an EQUINOX 1000 X-ray diffractometer operating with Co Kα radiation. The X-ray patterns were recorded every 0.030° in the range of $2\theta = 5°–100°$. The structural analyses and the particle size calculations, depending on strain of the particle, were revealed from XRD patterns.

The size and morphologies of the nanoparticles and the shell thicknesses of the coated nanoparticles were examined using a JEOL JEM-2010F high-resolution transmission electron microscope with high angle annular dark field (HAADF) detector operated at 200 kV. The nanoparticles diameters and the shell thicknesses were determined by statistical averaging using digital micrographs. The structural details of the nanoparticles were demystified using High Resolution TEM (HRTEM).

OA- and SiO_2-coated $ZnFe_2O_4$ were monitored with differential thermal and thermo gravimetric analysis (DT-TGA) employing TG/DTA 6300 model spectrometer under nitrogen flow at 40 mL/min with α-Al_2O_3 reference container. The heating rate employed was 10 °C/min in the temperature range of 30–800 °C.

Magnetization measurements were performed by means of the standard zero-field cooled (ZFC)–field-cooled (FC) procedures in the range of 5–300 K with applied fields of 500 Oe using a Quantum Design physical property measurement system (PPMS). The temperature dependence of the magnetization (*M–T*) and magnetic hysteresis (*M–H*) loops were also recorded using PPMS. EPR spectra of the prepared samples were recorded at the X band (∼9.8 GHz), using a Bruker EMX 131 spectrometer with 100 kHz magnetic field modulation. The EPR thermal study was performed in the temperature range of 120–400 K using a nitrogen gas-flow system.

Results and discussion

Figure 1 shows the XRD patterns of OA-coated and 13.0-nm SiO_2-coated $ZnFe_2O_4$ nanoparticles, in the 2θ range of 5°–100°. The patterns confirm the formation of single-phase (fcc) spinel structure of the prepared samples. The XRD patterns were compared and indexed using JCPDS file no (22-1012). This analysis revealed the single phase cubic spinel structure of $ZnFe_2O_4$ with *Fd*-3*m* space group. The XRD pattern of SiO_2-coated $ZnFe_2O_4$ is also shown in Fig. 1. Besides the highest peak originated from (311) of ferrite in the pattern, the XRD pattern of SiO_2-coated $ZnFe_2O_4$ nanoparticles presented a broad featureless XRD peak between 20° and 40° diffraction angles corresponding to the amorphous nature of SiO_2 shells. The crystallite size of synthesized OA-coated $ZnFe_2O_4$ nanoparticles were calculated from the full-width at half-maximum (FWHM) measurement from the prominent X-ray diffraction peaks using Scherrer's formula (Warren 1996). The average particle size was estimated to be about 5.89 ± 0.33 nm by the most intense (311) peak assuming that strain can be neglected.

Figure 2a shows the TEM image of uniform distribution of $ZnFe_2O_4$ nanoparticles, which are surface coated by OA. The particles were found to have a

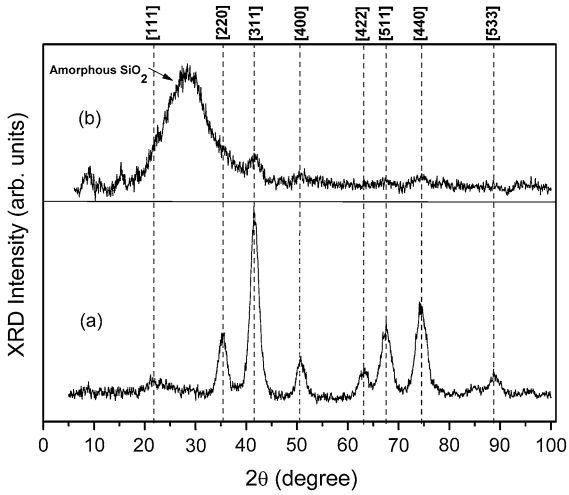

Fig. 1 XRD patterns of **a** OA and **b** 13.0-nm thick SiO_2-coated $ZnFe_2O_4$ nanoparticles

narrow-size distribution with an average size of 5.75 ± 0.75 nm which confirms the particle size obtained from XRD data, using Scherrer's formula (=5.89 nm). Figure 2b shows typical TEM image of core/shell nanoparticles with an average silica shell thickness of 13.0 nm with standard deviation of 0.68 nm. The other TEM images of core/shell nanoparticles with different SiO_2-shell thicknesses are not given here due to space limitations. Figure 2c shows the TEM-HAADF image of SiO_2-coated nanoparticles. The nanoparticles have a core/shell structure with the bright contrast corresponds to heavier ferrite nanoparticles and the dark contrast corresponds to light silica shells. As shown in the figure, most particles are spherical and have single core as well as some of the core nanoparticles are clustered together approved by HADDF image. In order to observe the detailed structure of SiO_2-coated $ZnFe_2O_4$ nanoparticles, HRTEM technique was used. HRTEM studies show that the amorphous SiO_2 shells completely cover the magnetic nanoparticles and have a "core/shell" structure with a clearly distinguishable interface. The image clearly shows the single crystallinity of $ZnFe_2O_4$ core and the amorphous nature of SiO_2 shell (Fig. 2d). The corresponding size distribution histograms and log-normal fitting analysis of OA coated and with a SiO_2 shell thickness of 13.0-nm $ZnFe_2O_4$ nanoparticles are shown in Fig. 3a, b, respectively. The results related to SiO_2 shell thickness depends on the amount of TEOS, and the calculated standard deviations for all samples are given in Table 1. It is seen that both particle size and SiO_2 shell thickness of the nanoparticles increase with increasing TEOS content. This result clearly demonstrates that the thickness of SiO_2 around the nanoparticles core can be easily controlled by simply varying the initial amount of TEOS (Lee et al. 2006; Hsieh et al. 2009).

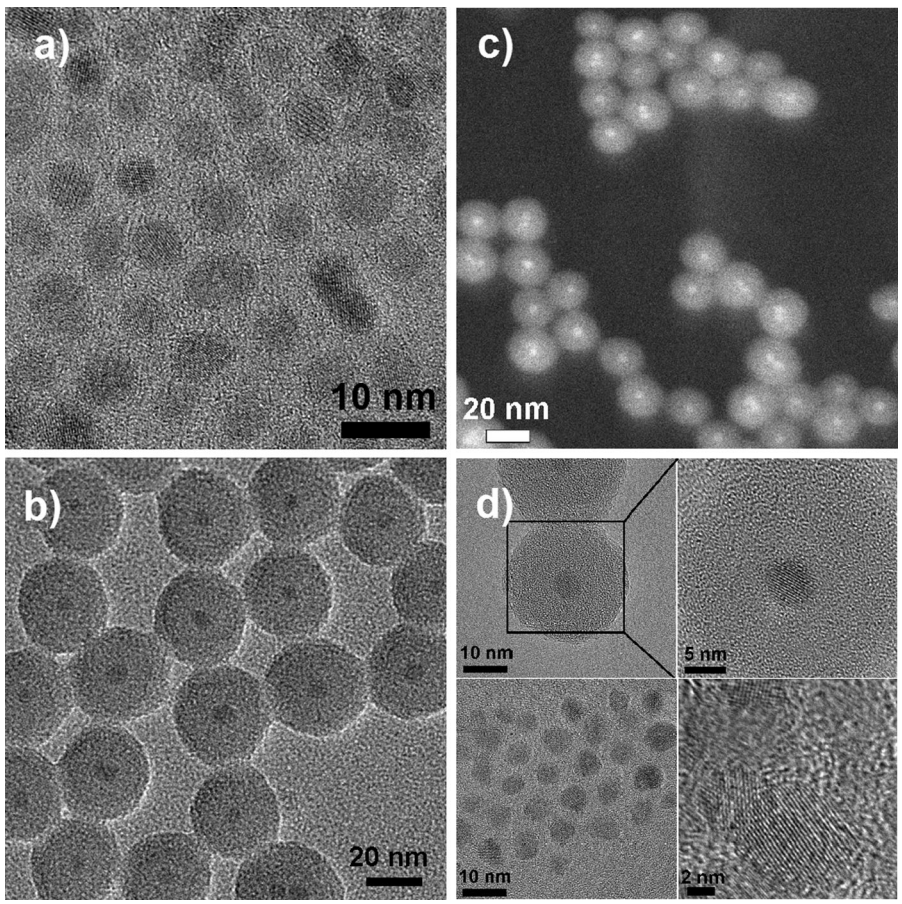

Fig. 2 **a** TEM image of OA-coated $ZnFe_2O_4$ nanoparticles, **b** TEM image and, **c** HAADF image of 13.0-nm thick silica-coated $ZnFe_2O_4$ nanoparticles and **d** an expanded view of a high resolution

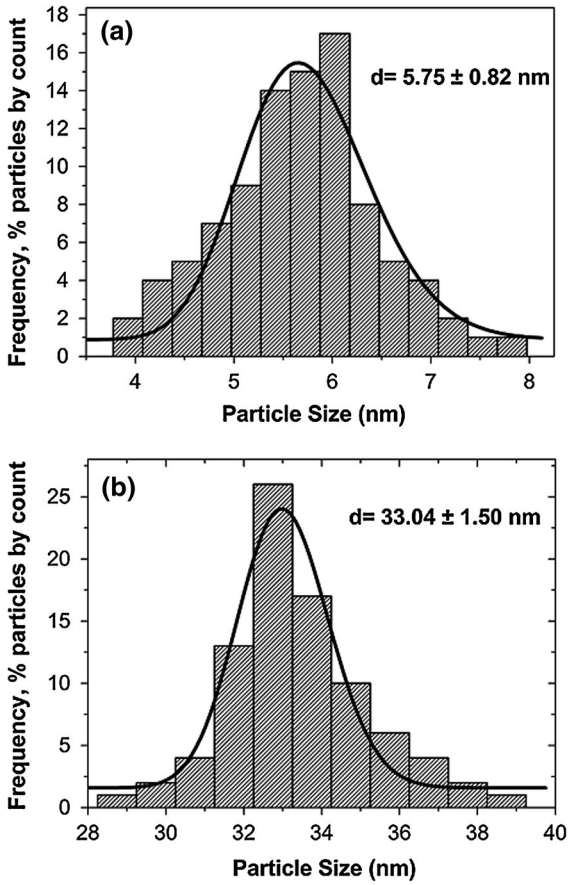

Fig. 3 Size distribution (*histogram*) of $ZnFe_2O_4$ nanoparticles from TEM images **a** OA and **b** 13.0-nm thick SiO_2-coated $ZnFe_2O_4$ nanoparticles

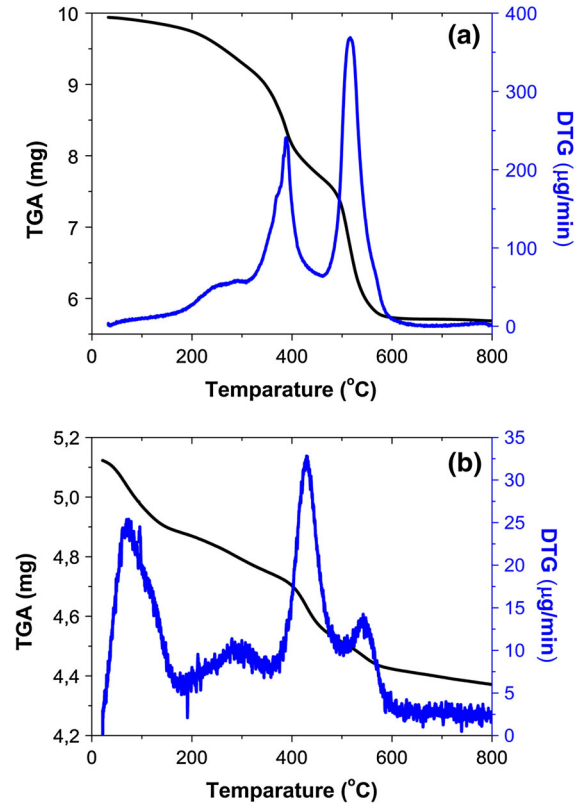

Fig. 4 TGA/DTG curves of $ZnFe_2O_4$ nanoparticles coated with **a** OA and **b** SiO_2

The mass losses under continous N_2 flow were monitored by TGA/DTG measurements for oleic acid and SiO_2 coated nanoparticles. The results are given in Fig. 4a, b. The first mass loss about 3.50 % was observed to occur in the temperature range between 30–200 °C due to evaporation of water, methanol, and ethanol for oleic acid coated nanoparticles (Ayyappan et al. 2008). The next mass loss (approximately 1.5 %) occurs in the temperature range of 236–250 °C due to evaporation temperature of diethylene glycol (DEG) which has an evaporation temperature of 244 °C. The two major mass losses about 5 % and 20 %, which are attributed to loosing second and first order bonded functional groups (COOH) around the nano particles were observed to occur at about 290–315 °C

Table 1 The average particle size from XRD and TEM

TEOS content (mL)	Scherrer's formula OA-coated (nm)	Determined from TEM figures		
		OA-coated (nm)	SiO_2-coated (nm)	Thickness of SiO_2 shell (nm)
0.00	5.89 ± 0.33	5.75 ± 0.75	–	–
0.25	–	–	21.62 ± 1.25	7.94 ± 0.46
0.50	–	–	24.18 ± 1.31	9.22 ± 0.50
1.00	–	–	27.95 ± 1.43	11.10 ± 0.57
1.50	–	–	31.78 ± 1.50	13.02 ± 0.62
2.50	–	–	33.94 ± 1.64	14.10 ± 0.68

and 315–500 °C, respectively. Similar results related with the first and second order mass loss originated from the breaking of bonded oleic acids to the ferrite nanoparticles were also reported in the earlier similar works (Ayyappan et al. 2008; Binder and Weinstabl 2007; Zhao et al. 2006). The most important mass loss occuring in the range of 500–600 °C was correlated to the phase transitions of iron atoms in the lattice ending with release of CO, CO_2 and H_2O gasses from the sample (Ayyappan et al. 2008).

A mass loss about 5 % in temperature range of 30–200 °C was also observed for SiO_2-coated $ZnFe_2O_4$ (Fig 4b) due to evaporation of water, methanol ($T_{evaporation}$ = 64.7 °C) and the other chemicals. Evaporations of OA ($T_{evaporation}$ = 360 °C) and Igepal CO-520 ($T_{evaporation}$ = 200–300 °C), which were used during the SiO_2 coating are believed to give rise to the mass loss observed in the temperature range of 420–440 °C. The phase transitions of Fe atoms in the ferrite nanoparticles produce a mass loss (about 1.5–2 %) observed in temperature range of 540–550 °C.

The magnetic properties of OA- and SiO_2-coated nanoparticles were analyzed using a Quantum Design PPMS with a VSM accessory. Comparative measurements of the hysteresis loops of both OA and 13.0-nm SiO_2-coated nanoparticles measured at 300, 50, and 5 K are given in Fig. 5a, b. It is seen that OA- and SiO_2-coated $ZnFe_2O_4$ nanoparticles exhibit superparamagnetic behavior. The magnetization values of OA and 13.0-nm SiO_2-coated $ZnFe_2O_4$ nanoparticles were determined to be equal to 63.0 and 1.5 emu/g, respectively, at 300 K as shown in Fig. 5a, b. The magnetizations of SiO_2-coated samples are much smaller than that of OA-coated nanoparticles. This originates from the fact that non-magnetic SiO_2 shells constitute 80 to 95 % of the mass of the samples. This result is in agreement with the estimation made form TEM observation. However the saturation magnetization OA- and SiO_2-coated $ZnFe_2O_4$ nanoparticles are bigger than that reported value of ~5 emu/g for bulk $ZnFe_2O_4$ (Clark and Evans 1997). This type of anomalously high magnetizations occur when the Fe^{3+} ions migrate to tetrahedral site giving raise to strong super exchange interaction (Ayyappan et al. 2010; Yao et al. 2007). The coercivities (Hc) were measured to be consistently less than 20 Oe and 40 Oe for OA- and SiO_2-coated $ZnFe_2O_4$ nanoparticles at 300 K, respectively. Thus, all samples exhibit superparamagnetic behavior. Room temperature magnetic

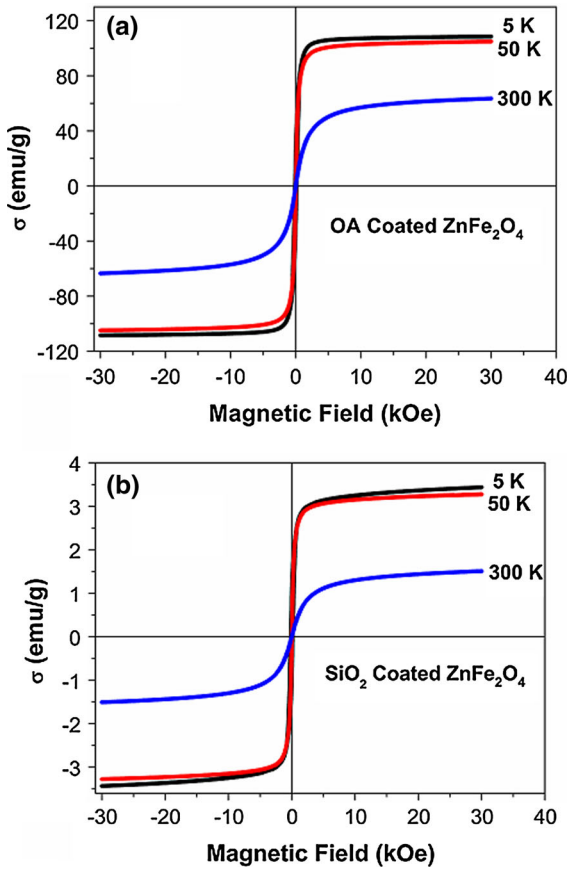

Fig. 5 Magnetization of **a** OA and **b** 13.0-nm thick SiO_2-coated $ZnFe_2O_4$ nanoparticles versus the magnetic field at 5, 50, and 300 K

properties determined by VSM method are given in Table 2 for prepared samples. These results indicate that non-magnetic SiO_2 coating layer on the surface of magnetic particles produced changes in the magnetism of studied samples (Zhao et al. 2008; Jiang et al. 2003). The only differences between OA- and SiO_2-coated $ZnFe_2O_4$ nanoparticles are the reduced saturation magnetization and slight increase in the coercivity fields of coated ones (Chang et al. 2010; Sotiriou et al. 2011). The fact that the amount of SiO_2 in a sample could not be determined precisely, and it was impossible to make the magnetization specific with respect to the amount of the cores. Consequently, the magnetic hysteresis loops of all samples were similar, indicating the negligible influence of SiO_2 coating on the magnetic properties.

Figure 6 shows the temperature-dependent ZFC and FC magnetization curves of OA and 13.0-nm

SiO_2-coated $ZnFe_2O_4$ nanoparticles, measured at an applied magnetic field of 500 Oe in the temperature range 5–300 K. The maximum of the ZFC curve is a characteristic of the average blocking temperature (T_B) of nanoparticles (Parma et al. 2012). Inspection of the ZFC curves given in Fig. 6 indicates that coating with 13.0-nm SiO_2 of the $ZnFe_2O_4$ nanoparticles causes a decrease in the T_B from 15.9 K to about 15.3 K. These values are in agreement with those reported in literature for SiO_2-coated magnetic nanoparticles (Zhang et al. 2012; Bumb et al. 2008). T_B values of $ZnFe_2O_4$ nanoparticles coated with SiO_2 shell of various thicknesses are given in Table 2. It is seen that the maximum T_B occurs at a SiO_2 coating thickness of about 8 nm. The T_B of the nanoparticles decreases with the increase in SiO_2 thickness. This effect of SiO_2 coating on blocking temperature has been well explained in our previous papers, published elsewhere on coated $NiFe_2O_4$ and $CoFe_2O_4$ nanoparticles (Coskun et al. 2012, 2010). In brief, it might due

Table 2 Summary of magnetic characteristics of samples: T_B, saturation magnetization (M_s), and coercivity (H_c)

TEOS content (mL)	Thickness of SiO_2 shell (nm)	T_B (K) ± 0.5 K	M_s (emu/g) ±0.2	Hc (Oe) ±5
0.00	–	15.9	63.0	18.0
0.25	7.94 ± 0.46	16.4	6.6	11.3
0.50	9.22 ± 0.50	16.0	5.0	16.5
1.00	11.10 ± 0.57	15.6	2.1	21.9
1.50	13.02 ± 0.62	15.3	1.5	37.0
2.50	14.10 ± 0.68	15.1	1.6	33.2

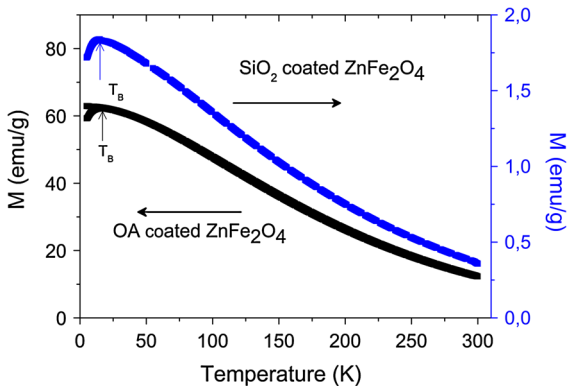

Fig. 6 Temperature dependence of the ZFC and FC magnetization measured at 500 Oe for OA- and SiO_2-coated $ZnFe_2O_4$ nanoparticles. The *arrows* indicate the T_B

to SiO_2 shell, which improves spin ordering at the surface, and reduces both magnetic dipole–dipole interaction and the average effective volume of $ZnFe_2O_4$ cores (Yao et al. 2007; Chang et al. 2010; Pereira et al. 2010).

EPR spectra of OA- and 13.0-nm SiO_2-coated $ZnFe_2O_4$ nanoparticles are given in Fig. 7. It is seen that the spectrum of OA-coated nanoparticles consists of two clearly distinguished components: a board asymmetric EPR line (signal 1) centered at the magnetic field of $H_R = 3{,}080$ G ($g = 2.01$) with a linewidth of $\Delta H_{pp} = 780$ G, and another asymmetric EPR line (signal 2) centered at the magnetic field of $H_R = 1{,}650$ G ($g = 4.3$) with a linewidth of $\Delta H_{pp} = 410$ G. The g-factor value 2.01 calculated for signal 1 from EPR measurement is in good agreement with that reported in the literature for nanostructured-$ZnFe_2O_4$ particles (Lin et al. 2006). This signal at $g = 2.01$ is likely due to Fe^{3+} ions staying in the octahedral symmetry sites in the spinel structure of the samples (Koksharov et al. 2001; Li et al. 2012). According to the signal assignment reported earlier, the weak signal centered at $g = 4.3$ is very specific and attributed to the isolated $^6S_{5/2}$ spin of Fe^{3+} ions in tetrahedral coordination with a strong rhombic distortion (Li et al. 2012; Hsieh and Lue 2002; Shafi et al. 1997; Noginova et al. 2008) and to an impurity of Fe_2O_3 at an EPR detectable level in OA-coated $ZnFe_2O_4$ sample (Shafi et al. 1998; Cao and Gu 2005). Variations of three EPR parameters with temperature of OA-coated $ZnFe_2O_4$ nanoparticles in the range of 120–400 K are given in Fig. 8. These parameters are the amplitude of the line (I_{PP}) (top panel), the resonance field (H_R) (middle panel), and the linewidth (ΔH_{pp}) (bottom panel) (see Fig. 8). As it is easily seen studied, parameters depend strongly on temperature. Temperature dependences of the resonance field H_R and of the linewidth ΔH_{pp} are very similar to those reported for other nanoparticle systems (Guskos et al. 2012), i.e., ΔH_{pp} increases as the temperature decreases and the resonance field shifts toward the lower magnetic field with decrease in temperature. These variations of the EPR line parameter were considered as a revelation of superparamagnetic regime of the ferrite nanoparticle spin system (Guskos et al. 2010). The amplitude of the line increases with decreasing temperature from 400 K, reaching a maximum value at about 200 K. Below this temperature, the line amplitude falls down with the

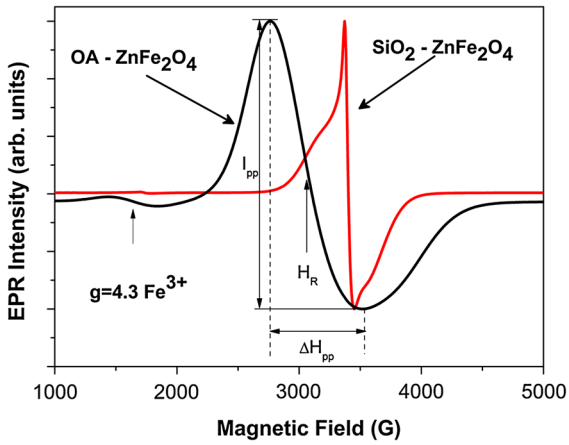

Fig. 7 ESR spectra of OA- and SiO_2-coated $ZnFe_2O_4$ nanoparticles measured at 300 K

temperature decrease (Guskos et al. 2012). Such a behavior of the resonance line intensity is a characteristic for the agglomeration of magnetic nanoparticles (Guskos et al. 2007, 2008).

Figure 9 shows EPR spectra of SiO_2-coated $ZnFe_2O_4$ nanoparticles obtained for different TEOS contents at 300 K. From the line fitting analysis it was concluded that the EPR spectrum of SiO_2-coated samples consists of a superposition of two resonance lines, a broad line associated with the particle-core contribution, and a narrow one associated with the particle-shell contribution at the center of the main signal appearing at about $g = 2.01$ (Koksharov et al. 2001; Berger et al. 2000; Vargas et al. 2008). Such a phenomenon, which is described in earlier works (Noginova et al. 2008, 2007), is typical for superparamagnetic nanoparticles embedded in a non-magnetic matrix (especially in diluted magnetic nanoparticle systems).

We also studied the effect of temperature on different spectrum parameters of SiO_2-coated $ZnFe_2O_4$ nanoparticles by EPR spectroscopy in the temperature range of 120–400 K. Experimental spectra recorded at each temperature were simulated by assuming the existence of two superimposed resonance lines of Gaussian shape with different line characteristics. The results of such a calculation using the data of an experimental EPR spectrum recorded at 300 K for 13.3 nm SiO_2-coated $ZnFe_2O_4$ nanoparticles is given in Fig. 10. It is seen that a model based on the presence of two resonance lines exhibiting different characteristics describes very well experimental spectra recorded at 300 K. Such a spectrum simulation

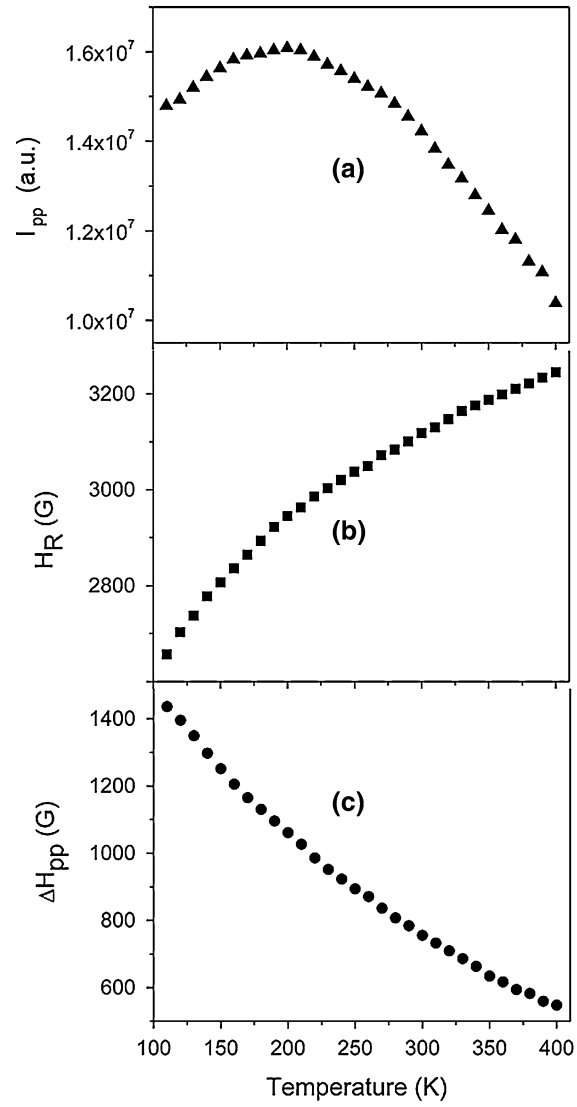

Fig. 8 The temperature dependence of the EPR parameters for OA-coated $ZnFe_2O_4$ nanoparticles **a** intensity (I_{PP}), **b** resonance field (H_R), and **c** linewidth (ΔH_{pp})

calculations were performed over the temperature range of 150–400 K, and characteristic parameters of the contributing resonance lines were calculated at each measured temperature. The results are given in Fig. 11a–c for 13-nm SiO_2-coated nanoparticles. The temperature dependence data derived in the present work for H_R and ΔH_{pp} parameters of the contributing broad resonance line are found to be very similar to those reported previously for other nanoparticles in that H_R decreases and ΔH_{pp} increases as the temperature decreases (Noginova et al. 2008, 2007; Parekh

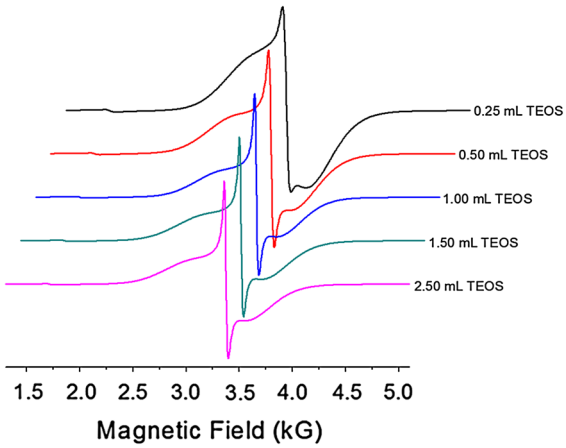

Fig. 9 300 K EPR spectra of $SiO_2/ZnFe_2O_4$ nanoparticles coated with different thickness in the presence of different TEOS content

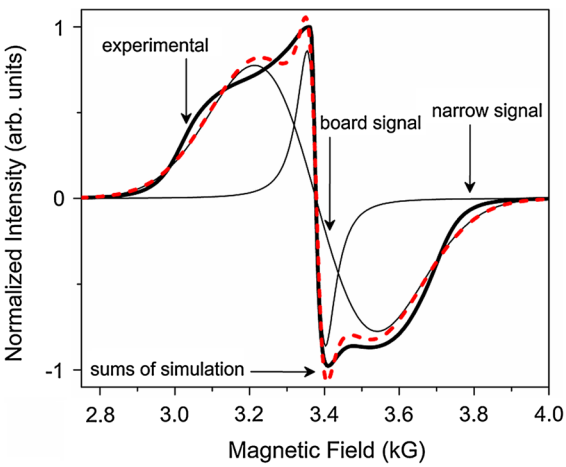

Fig. 10 Experimental and fitted EPR spectra at room temperature for 13.0-nm thick SiO_2-coated sample. The spectra are seen to be composed of two signals, viz., one intense and broad signal and one narrow signal

et al. 2000). The broadening and the shift of the resonance lines to lower magnetic fields with the decrease in temperature are the typical behaviors of superparamagnetic nanoparticles reported in the literature (Cao and Gu 2005; Vargas et al. 2008). For ideal paramagnetic systems, I_{pp} is expected to be proportional to the paramagnetic susceptibility. This is the case for contributing broad line which exhibits the superparamagnetic-core characteristics (Vargas et al. 2008). As for the narrow line, its intensity and ΔH_{pp} remain almost constant down to 170 K while it is resonance field (H_R) increases monotonically with decrease in temperature. Such narrow resonance lines

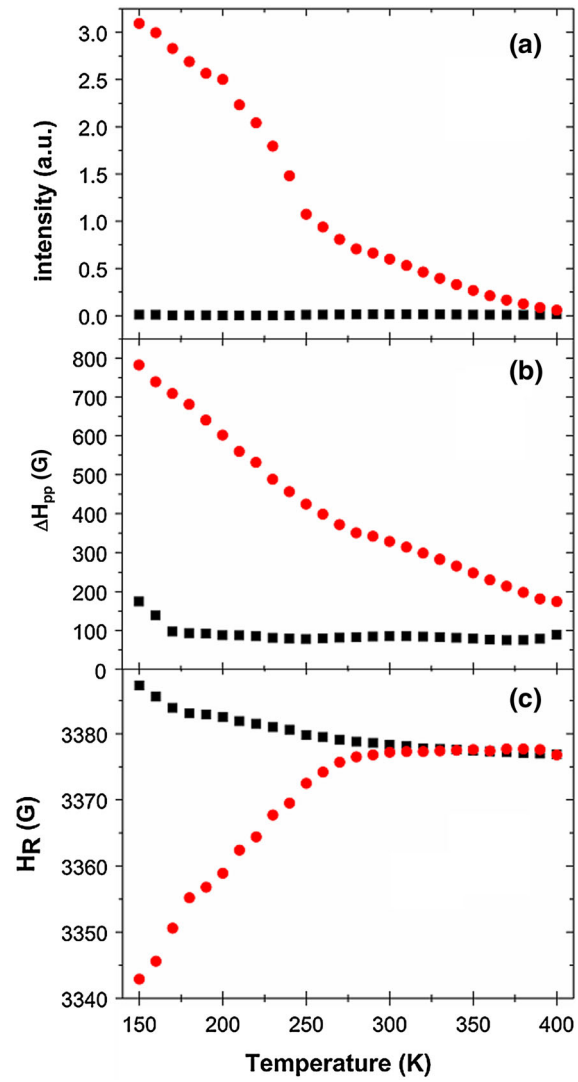

Fig. 11 Variations with temperature of the characteristic parameters of the contributing resonance lines determined from spectrum simulation calculations for SiO_2-coated $ZnFe_2O_4$ nanoparticles. **a** intensity (I_{PP}), **b** linewidth (ΔH_{pp}), and **c** resonance field (H_R) (*circles* board line, *squares* narrow line)

were also observed in core/shell nanostructures indicating the presence of free radicals on silica shell due to the presence of dangling bonds in the silica (Vaidya et al. 2011). Variations with temperature of the I_{pp}, ΔH_{pp}, and H_R parameters of the resonance line appearing at $g = 3.97$ of SiO_2-coated nanoparticles were also studied (not given here). It is found that investigated parameters exhibit temperature dependences similar to those obtained for OA-coated nanoparticles.

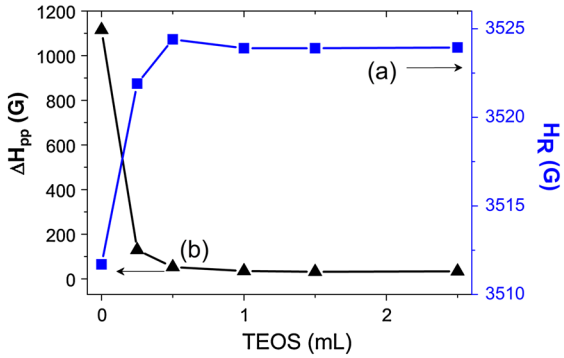

Fig. 12 TEOS contents dependence of the EPR H_R and H_{pp} parameters of $ZnFe_2O_4$ nanoparticles **a** resonance field (H_R), **b** linewidth (ΔH_{pp})

Dependences of the EPR signal H_R and ΔH_{pp} parameters on TEOS content were also investigated at 300 K for OA and SiO_2-coated $ZnFe_2O_4$ nanoparticles by taking the board lines into account. The results of this study are given in Fig. 12. ΔH_{pp} parameter of SiO_2-coated nanoparticles was observed to be smaller than that obtained for OA-coated nanoparticles. As it seen from Fig. 12 while ΔH_{pp} decreases with the increase in the TEOS content and the line shifts toward higher magnetic fields. H_R continues to increase up to 0.5 mL TEOS content and then remains nearly constant in the range of 0.5–2.5 mL TEOS content. ΔH_{pp} decreases significantly (1,000 G) with the increase in TEOS content first, then remains almost constant in the TEOS content range of 0.5–2.5 mL. This sharp decrease in ΔH_{pp} parameter is attributed to the increased non-magnetic silica shell thickness on $ZnFe_2O_4$ core and to the decrease in the dipole–dipole interaction. These results obviously demonstrate that EPR parameters of SiO_2-coated $ZnFe_2O_4$ nanoparticles are strongly influenced by the silica shell thickness (Hsieh et al. 2009).

Conclusion

In the present work, the magnetic properties of OA- and SiO_2-coated $ZnFe_2O_4$ core/shell nanoparticles were investigated using different analysis techniques. The influence of SiO_2 shell thickness on the magnetic properties was also analyzed. The results of XRD and TEM analyses proved that the particle size of SiO_2-coated $ZnFe_2O_4$ nanoparticles ranged from ~22 to 34 nm in diameter with a magnetic core of ~6 nm, which increased with the increase in TEOS content. Magnetic properties of OA- and SiO_2-coated nanoparticles were investigated in detail to clarify the effect of silica coating on the T_B. SiO_2-coated $ZnFe_2O_4$ nanoparticles were found to exhibit superparamagnetic behavior in the investigated temperature range. The experimental results showed that due to the existence of a non-magnetic silica layer and good dispersion of $ZnFe_2O_4$ core particles in the SiO_2 matrix, the saturation magnetization of the silica-coated nanoparticles decreased as TEOS content increased. It is found that at the beginning of SiO_2 shells coating of $ZnFe_2O_4$ nanoparticles in the range of 7–14 nm cause an increase in the T_B. However, after certain coating thickness, due to surface anisotropy and magnetic interparticle interaction, T_B starts to decrease. The effect on the T_B of decreased magnetic interparticle interactions was also investigated by EPR technique using nanoparticle coated with SiO_2 of different thickness. Variations with temperature of the EPR spectrum characteristics of OA- and SiO_2-coated $ZnFe_2O_4$ nanoparticles were also reported in the present works. The main differences between OA- and SiO_2-coated $ZnFe_2O_4$ nanoparticles were observed to arise from surface environments and magnetic interparticle interactions.

SiO_2 surfaces are chemically stable and biocompatible. Therefore, SiO_2-coated ferrite nanoparticles prepared by the technique presented in this work have great potential applications in various biomedical fields, such as targeted drug delivery and magnetic hyperthermia.

Acknowledgments The authors would like to thank Dr. S. Ismat Shah for giving an opportunity to take TEM micrographs and Superconductivity and Nano Technology Group (SNTG) for PPMS and XRD measurements.

References

Ahmad T, Bae H, Rhee I, Chang Y, Jin SU, Hong S (2012) Gold-coated iron oxide nanoparticles as a T-2 contrast agent in magnetic resonance imaging. J Nanosci Nanotechnol 12:5132–5137

Ayyappan S, Gnanaprakash G, Panneerselvam G, Antony MP, Philip J (2008) Effect of surfactant monolayer on reduction of Fe_3O_4 nanoparticles under vacuum. J Phys Chem C 112:18376–18383

Ayyappan S, Raja SP, Venkateswaran C, Philip J, Raj B (2010) Room temperature ferromagnetism in vacuum annealed $ZnFe_2O_4$ nanoparticles. Appl Phys Lett 96:143106

Bayal N, Jeevanandam P (2012) Synthesis of CuO@NiO core–shell nanoparticles by homogeneous precipitation method. J Alloy Compd 537:232–241

Berger R, Kliava J, Bissey JC, Baietto V (2000) Magnetic resonance of superparamagnetic iron-containing nanoparticles in annealed glass. J Appl Phys 87:7389–7396

Binder WH, Weinstabl HC (2007) Surface-modified Superparamagnetic Ironoxide Nanoparticles. Monatshefte Fur Chemie 138:315–320

Bumb A, Brechbiel MW, Choyke PL, Fugger L, Eggeman A, Prabhakaran D, Hutchinson J, Dobson PJ (2008) Synthesis and characterization of ultra-small superparamagnetic iron oxide nanoparticles thinly coated with silica. Nanotechnology 19(33):335601

Cao XB, Gu L (2005) Spindly cobalt ferrite nanocrystals: preparation, characterization and magnetic properties. Nanotechnology 16:180–185

Carter CB, Norton MG (2007) Ceramic materials: science and engineering. Springer, New York

Caruntu D, Remond Y, Chou NH, Jun MJ, Caruntu G, He JB, Goloverda G, O'Connor C, Kolesnichenko V (2002) Reactivity of 3D transition metal cations in diethylene glycol solutions. Synthesis of transition metal ferrites with the structure of discrete nanoparticles complexed with long-chain carboxylate anions. Inorg Chem 41:6137–6146

Caruntu D, Caruntu G, Chen Y, O'Connor CJ, Goloverda G, Kolesnichenko VL (2004) Synthesis of variable-sized nanocrystals of Fe_3O_4 with high surface reactivity. Chem Mater 16:5527–5534

Caruntu D, Caruntu G, O'Connor CJ (2007) Magnetic properties of variable-sized Fe_3O_4 nanoparticles synthesized from non-aqueous homogeneous solutions of polyols. J Phys D 40:5801–5809

Chakka VM, Altuncevahir B, Jin ZQ, Li Y, Liu JP (2006) Magnetic nanoparticles produced by surfactant-assisted ball milling. J Appl Phys 99:08E912

Chang C-C, Zhao L, Wu M-K (2010) Magnetodielectric study in SiO_2-coated Fe_3O_4 nanoparticle compacts. J Appl Phys 108:094105

Clark TM, Evans BJ (1997) Enhanced magnetization and cation distributions in nanocrystalline $ZnFe_2O_4$: a conversion electron Mossbauer spectroscopic investigation. IEEE Trans Magn 33:3745–3747

Coskun M, Korkmaz M, Firat T, Jaffari GH, Shah SI (2010) Synthesis of SiO_2 coated $NiFe_2O_4$ nanoparticles and the effect of SiO_2 shell thickness on the magnetic properties. J Appl Phys 107:09B523

Coskun M, Can MM, Coskun OD, Korkmaz M, Firat T (2012) Surface anisotropy change of $CoFe_2O_4$ nanoparticles depending on thickness of coated SiO_2 shell. J Nanopart Res 14:1–9

Deng YH, Wang CC, Hu JH, Yang WL, Fu SK (2005) Investigation of formation of silica-coated magnetite nanoparticles via sol–gel approach. Coll Surf A 262:87–93

Deraz NM, Alarifi A (2012) Microstructure and magnetic studies of zinc ferrite nano-particles. Int J Electrochem Sci 7:6501–6511

Gatelyte A, Jasaitis D, Beganskiene A, Kareiva A (2011) Sol–gel synthesis and characterization of selected transition metal nano-ferrites. Mater Sci-Medziagotyra 17(3):302–307

Ghiaci M, Valikhani D, Sadeghi Z (2012) Synthesis and characterization of silica-supported Pd nanoparticles and its application in the Heck reaction. Chin Chem Lett 23:887–890

Guskos N, Maryniak M, Typek J, Pelech I, Narkiewicz U, Roslaniec Z, Kwiatkowska M (2007) Temperature dependence of the FMR spectra of polymer composites with nanocrystalline alpha-Fe/C filler. Doped Nanopowders 128:213–218

Guskos N, Zolnierkiewicz G, Guskos A, Typek J, Blyszko J, Kiernozycki W, Narkiewicz U, Podsiadly M (2008) Magnetic properties of the micro-silica/cement matrix with carbon-coated cobalt nanoparticles and free radical DPPH. J Non-Cryst Solids 354:4510–4514

Guskos N, Zolnierkiewicz G, Typek J, Orlowski M, Guskos A, Czech Z, Mickiewicz A (2010) FMR study of gamma-Fe_2O_3 agglomerated nanoparticles in glue. Rev Adv Mater Sci 23:70–75

Guskos N, Glenis S, Zolnierkiewicz G, Typek J, Berczynski P, Guskos A, Sibera D, Narkiewicz U (2012) Magnetic properties of $ZnFe_2O_4$ ferrite nanoparticles embedded in ZnO matrix. Appl Phys Lett 100:122403

Hagura N, Widiyastuti W, Iskandar F, Okuyama K (2010) Characterization of silica-coated silver nanoparticles prepared by a reverse micelle and hydrolysis-condensation process. Chem Eng J 156:200–205

Han D, Luo H, Yang Z (1996) Remanent and anisotropic switching field distribution of platelike Ba-ferrite and acicular particulate recording media. J Magn Magn Mater 161:376–378

Hsieh CT, Lue JT (2002) Anisotropy-induced quantum critical behavior of magnetite nanoparticles at low temperatures. Phys Lett A 300:636–640

Hsieh TH, Ho KS, Bi XT, Han YK, Chen ZL, Hsu CH, Chang YC (2009) Synthesis and electromagnetic properties of polyaniline-coated silica/maghemite nanoparticles. Eur Polym J 45:613–620

Jiang HY, Zhong W, Tang NJ, Liu XS, Du YW (2003) Chemical synthesis of highly magnetic, air-stable silica-coated iron particles. Chin Phys Lett 20:1855–1857

Joo SH, Park JY, Tsung C-K, Yamada Y, Yang P, Somorjai GA (2009) Thermally stable Pt/mesoporous silica core-shell nanocatalysts for high-temperature reactions. Nat Mater 8:126–131

Kim D-H, Nikles DE, Brazel CS (2010) Synthesis and characterization of multifunctional chitosan-$MnFe_2O_4$ nanoparticles for magnetic hyperthermia and drug delivery. Materials 3(7):4051–4065

Kobayashi Y, Katakami H, Mine E, Nagao D, Konno M, Liz-Marzan LM (2005) Silica coating of silver nanoparticles using a modified Stober method. J Coll Interface Sci 283:392–396

Koksharov YA, Pankratov DA, Gubin SP, Kosobudsky ID, Beltran M, Khodorkovsky Y, Tishin AM (2001) Electron paramagnetic resonance of ferrite nanoparticles. J Appl Phys 89:2293–2298

Lee DC, Mikulec FV, Pelaez JM, Koo B, Korgel BA (2006) Synthesis and magnetic properties of silica-coated FePt nanocrystals. J Phys Chem B 110:11160–11166

Lee J, Lee Y, Youn JK, Bin Na H, Yu T, Kim H, Lee SM, Koo YM, Kwak JH, Park HG, Chang HN, Hwang M, Park JG, Kim J, Hyeon T (2008) Simple synthesis of functionalized superparamagnetic magnetite/silica core/shell nanoparticles and their application as magnetically separable high-performance biocatalysts. Small 4:143–152

Li B, Xu J, Liu J, Zuo S, Pan Z, Wu Z (2012) Preparation of mesoporous ferrisilicate with high content of framework iron by pH-modification method and its catalytic performance. J Coll Interface Sci 366(1):114–119

Lin L, Hsu KH, Lin JG (2006) Doping effects on the magnetic resonance of $ZnFe_2O_4$ and $NiFe_2O_4$. J Magn Magn Mater 304(1):e467–e469

Lopez J, Gonzalez-Bahamon LF, Prado J, Caicedo JC, Zambrano G, Gomez ME, Esteve J, Prieto P (2012) Study of magnetic and structural properties of ferrofluids based on cobalt-zinc ferrite nanoparticles. J Magn Magn Mater 324:394–402

Lu A, Salabas E, Schuth F (2007) Magnetic nanoparticles: synthesis, protection, functionalization, and application. Angewandte Chemie 46:1222–1244

Ma R, Levard C, Marinakos SM, Cheng YW, Liu J, Michel FM, Brown GE, Lowry GV (2012) Size-controlled dissolution of organic-coated silver nanoparticles. Environ Sci Technol 46:752–759

Madrakian T, Afkhami A, Zolfigol MA, Ahmadi M, Koukabi N (2012) Application of modified silica coated magnetite nanoparticles for removal of iodine from water samples. Nano Micro Lett 4:57–63

Moumen N, Pileni MP (1996) New syntheses of cobalt ferrite particles in the range 2–5 nm: comparison of the magnetic properties of the nanosized particles in dispersed fluid or in powder form. Chem Mater 8(5):1128–1134

Murai K, Watanabe Y, Saito Y, Nakayama T, Suematsu H, Jiang W, Yatsui K, Shim KH, Niihara K (2007) Preparation of copper nanoparticles with an organic coating by a pulsed wire discharge method. J Ceram Process Res 8:114–118

Nalbandian L, Delimitis A, Zaspalis VT, Deliyanni EA, Bakoyannakis DN, Peleka EN (2008) Hydrothermally prepared nanocrystalline Mn–Zn ferrites: synthesis and characterization. Microporous Mesoporous Mater 114:465–473

Noginova N, Chen F, Weaver T, Giannelis EP, Bourlinos AB, Atsarkin VA (2007) Magnetic resonance in nanoparticles: between ferro- and para-magnetism. J Phys Condens Matter 19:246208

Noginova N, Weaver T, Giannelis EP, Bourlinos AB, Atsarkin VA, Demidov VV (2008) Observation of multiple quantum transitions in magnetic nanoparticles. Phys Rev B 77(1):014403

Parekh K, Upadhyay RV, Mehta RV, Srinivas D (2000) Electron spin resonance study of a temperature sensitive magnetic fluid. J Appl Phys 88:2799–2804

Parma A, Freris I, Riello P, Cristofori D, Fernandez CDJ, Amendola V, Meneghetti M, Benedetti A (2012) Structural and magnetic properties of mesoporous SiO_2 nanoparticles impregnated with iron oxide or cobalt-iron oxide nanocrystals. J Mater Chem 22:19276–19288

Pereira C, Pereira AM, Quaresma P, Tavares PB, Pereira E, Araujo JP, Freire C (2010) Superparamagnetic gamma-Fe_2O_3@SiO_2 nanoparticles: a novel support for the immobilization of VO(acac)(2). Dalton Trans 39(11):2842–2854

Quarta A, Curcio A, Kakwere H, Pellegrino T (2012) Polymer coated inorganic nanoparticles: tailoring the nanocrystal surface for designing nanoprobes with biological implications. Nanoscale 4:3319–3334

Selvan ST (2010) Silica-coated quantum dots and magnetic nanoparticles for bioimaging applications (Mini-Review). Biointerphases 5:FA110–FA115

Shafi K, Koltypin Y, Gedanken A, Prozorov R, Balogh J, Lendvai J, Felner I (1997) Sonochemical preparation of nanosized amorphous $NiFe_2O_4$ particles. J Phys Chem B 101(33):6409–6414

Shafi K, Gedanken A, Prozorov R, Balogh J (1998) Sonochemical preparation and size-dependent properties of nanostructured $CoFe_2O_4$ particles. Chem Mater 10:3445–3450

Sotiriou GA, Hirt AM, Lozach P-Y, Teleki A, Krumeich F, Pratsinis SE (2011) Hybrid, silica-coated, janus-like plasmonic-magnetic nanoparticles. Chem Mater 23:1985–1992

Soundarya N, Zhang Y (2010) Use of core–shell structured nanoparticles for biomedical applications. Recent Pat Biomed Eng 1(1):34–42

Tung LD, Kolesnichenko V, Caruntu G, Caruntu D, Remond Y, Golub VO, O'Connor CJ, Spinu L (2002) Annealing effects on the magnetic properties of nanocrystalline zinc ferrite. Physica B Condens Matter 319:116–121

Vaidya S, Thaplyal P, Ramanujachary KV, Lofland SE, Ganguli AK (2011) Synthesis of core–shell nanostructures of Co_3O_4@SiO_2 with controlled shell thickness (5–20 nm) and hollow shells of silica. J Nanosci Nanotechnol 11:3405–3413

Vargas JM, Lima E, Zysler RD, Duque JGS, De Biasi E, Knobel M (2008) Effective anisotropy field variation of magnetite nanoparticles with size reduction. Eur Phys J B 64:211–218

Wang JF, Tsuzuki T, Sun L, Wang XG (2010) Reverse microemulsion-mediated synthesis of SiO_2-coated ZnO composite nanoparticles: multiple cores with tunable shell thickness. ACS Appl Mater Interfaces 2:957–960

Wang Y-F, Fu C-M, Chuang M-H, Cham T-M, Chung M-I (2011) Magnetically directed targeting aggregation of radiolabelled ferrite nanoparticles. J Nanomater. doi:10.1155/2011/851520

Warren BE (1996) X-Ray Diffraction. Addison-Wesley, Boston

Wu S, Sun AZ, Xu WH, Zhang Q, Zhai FQ, Logan P, Volinsky AA (2012) Iron-based soft magnetic composites with Mn–Zn ferrite nanoparticles coating obtained by sol–gel method. J Magn Magn Mater 324:3899–3905

Xu Y, Liang YT, Jiang LJ, Wu HR, Zhao HZ, Xue DS (2011) Preparation and magnetic properties of $ZnFe_2O_4$ nanotubes. J Nanomater. doi:10.1155/2011/525967

Yanez-Vilar S, Sanchez-Andujar M, Gomez-Aguirre C, Mira J, Senaris-Rodriguez MA, Castro-Garcia S (2009) A simple solvothermal synthesis of MFe_2O_4 (M = Mn, Co and Ni) nanoparticles. J Solid State Chem 182:2685–2690

Yao C, Zeng Q, Goya GF, Torres T, Liu J, Wu H, Ge M, Zeng Y, Wang Y, Jiang JZ (2007) $ZnFe_2O_4$ nanocrystals: synthesis and magnetic properties. J Phys Chem C 111(33):12274–12278

Zhang XF, Mansouri S, Clime L, Ly HQ, Yahia LH, Veres T (2012) Fe_3O_4-silica core-shell nanoporous particles for high-capacity pH-triggered drug delivery. J Mater Chem 22:14450–14457

Zhao SY, Lee DK, Kim CW, Cha RG, Kim YH, Kang YS (2006) Synthesis of magnetic nanoparticles of Fe_3O_4 and $CoFe_2O_4$ and their surface modification by surfactant adsorption. Bull Korean Chem Soc 27:237–242

Zhao XL, Shi YL, Wang T, Cai YQ, Jiang GB (2008) Preparation of silica-magnetite nanoparticle mixed hemimicelle sorbents for extraction of several typical phenolic compounds from environmental water samples. J Chromatogr A 1188:140–147